

Adsorption of molecular oxygen on the walls of pristine and carbon-doped (5,5) boron nitride nanotubes: Spin-polarized density functional study

Jia Zhang,^{1,2} Kian Ping Loh,^{1,*} Jianwei Zheng,² Michael B. Sullivan,² and Ping Wu²

¹*Department of Chemistry, National University of Singapore, 3 Science Drive 3, Singapore 117543, Singapore*

²*Institute of High Performance Computing, Capricorn, Singapore Science Park II, Singapore 117528, Singapore*

(Received 15 December 2006; revised manuscript received 14 February 2007; published 5 June 2007)

We performed *ab initio* calculations to study the effect of molecular oxygen adsorption on the electronic properties of (5,5) pristine and carbon-doped boron nitride (BN) nanotube. The binding energies of oxygen molecules physisorbed at different sites were determined by considering both short- and long-range interactions. Spin-polarized calculation within the density functional theory yielded the triplet ground state for oxygen physisorbed on pure BN nanotube; the large energy gap between the unoccupied oxygen levels and the top of the valence band indicates the absence of hole doping. The introduction of substitutional carbon impurity increases the reactivity of BN nanotube toward molecular oxygen and stable O₂ chemisorption states exist on both carbon-substituted nitrogen site (C_N) and carbon-substituted boron site (C_B) defect sites. Chemisorbed O₂ on the C_N defect is found to impart metallicity on the BN nanotube.

DOI: [10.1103/PhysRevB.75.245301](https://doi.org/10.1103/PhysRevB.75.245301)

PACS number(s): 81.07.De, 82.20.Wt, 73.20.At, 79.60.Jv

I. INTRODUCTION

Boron nitride (BN) nanotubes, the III-V analog of carbon nanotubes, can be produced using chemical-vapor deposition methods, although its mass production is not widespread.¹ Possible applications which take advantage of its lightweight and polar-BN bonds include hydrogen storage and piezoelectric materials.^{2,3} Due to its wide band gap, the electronic properties of BN nanotubes can be dependent on the diameter and chirality of the tube.⁴ Calculations showed that for BN nanotubes with diameters of 5 nm or more, a sizable gap reduction should be achievable with the application of transverse electrical fields, such band-gap tuning is more amenable in BN nanotubes compared to carbon nanotube.⁵ Besides external electrical field tuning, the insulating tube can be doped to make it a semiconductor. It is important to study the effect of exohedral doping on the electronic properties of these nanotubes, these have implications for the use of nanotubes as gas sensors, or in transistors where the presence of polar adsorbates may create a screening field for electrical voltages applied to the tube.⁶ Chemical functionalization of the tubes at localized sites can change the *sp*²- to *sp*³-type bonding and open up the band gap of small-gap nanotube.⁷ The exohedral doping of boron nitride nanotube (BNNT) by chemical adsorption of atomic species on the tube walls have been previously considered.⁸ Results suggest that hole doping is induced by adsorption of atomic H species on the B site. Besides hydrogen, the oxygenation of nanotube can influence the electrical, dielectric, and magnetic properties. Experiments have shown that the electrical conductance of single-walled semiconducting carbon nanotubes is extremely sensitive to exposure to oxygen. For instance, small-gap carbon nanotube becomes metallic when they are exposed to oxygen.⁹ Nuclear magnetic resonance showed that spin relaxation rate for carbon nanotubes changed significantly in the presence of oxygen, suggesting that physisorbed triplet O₂ affect the magnetic property.¹⁰ Spin-unpolarized calculations based on local-density approximation (LDA) predicted that the semiconducting carbon nanotube becomes metallic

with O₂ physisorption;¹¹ however, a later spin-polarized calculation using generalized gradient approximation (GGA) showed that hole doping of carbon nanotube by physisorbed O₂ is not valid because of the energy gap of 0.5 eV between the empty oxygen spin-down state and the valence-band maximum.¹² It was suggested that the main effect of oxygen was not to dope the tubes but to modify the barriers of metal-semiconductor contact.

In this paper, we presented a detailed first-principles analysis of O₂ adsorption on pristine (5,5) BN nanotubes and carbon-doped BN nanotubes, using both spin-polarized and unpolarized calculation. It is known that BN nanotube is more resistant to oxidation compared to carbon nanotube, so it is interesting to consider pathways where BN nanotube can be oxygenated. It is plausible that such oxygenation proceeds via defect sites on the BN nanotube. During chemical-vapor deposition, intentionally or otherwise, carbon atom can substitute for boron or nitrogen atoms in the nanotube to produce a BCN hybrid, the presence of such defects may impart increased reactivity to oxygen. In this case, a charge transfer may occur between the oxygen and carbon-doped BN nanotube, which in turn induces hole-doping effects in the nanotube. A previous study shows that carbon-doped BN has a doublet ground state and localized magnetism due to carbon 2*p* electron;¹³ it is interesting to consider the effect produced by oxygen chemisorption on the magnetic properties.

II. METHODS OF CALCULATION

Density functional theory (DFT) calculations were performed using the Vienna *ab initio* simulation package (VASP).¹⁴ The electron-ion interaction was modeled using the projector-augmented wave method.^{15,16} Both spin-unpolarized and spin-polarized GGA scheme was used for the exchange and correlation functions.¹⁷ The cutoff energy was set to 400 eV. To calculate the atomic and electronic structures of oxidized BN nanotube, supercells of four BN layers for the defect-free (5, 5) BNNT were chosen with 20 B and 20 N atoms in one supercell. Periodic boundary con-

TABLE I. Adsorption energies and equilibrium O₂-tube distances for the adsorption of O₂ on pristine (5,5) BN nanotube. The superscripts “b” and “n” in column 3 indicate $d_{\text{B-O}}$ and $d_{\text{N-O}}$, respectively. $E_b = E_a + E_{\text{vdw}}$.

Site	Spin state	$d_{\text{B-O,N-O}}$ (Å)	E_a (meV)/O ₂	E_{vdw} (meV)/O ₂	E_b (meV)/O ₂
B	Spin unpolarized	3.27 ^b	897		
B	Singlet	3.27 ^b	407		
B	Triplet	3.27 ^b	-27.8	-58.5	-86.3
N	Singlet	3.33 ⁿ	407		
N	Triplet	3.33 ⁿ	-27.4	-58.4	-85.8
P	Spin unpolarized		915		
P	Triplet	3.02, ^b 3.24 ⁿ	2.3	-70.5	-68.2
T	Singlet	3.10, ^b 3.36 ⁿ	425		
T	Triplet	3.10, ^b 3.36 ⁿ	-3.5	-68.9	-72.4

dition along the BN nanotube axis direction was employed with a vacuum region of 12 Å between the tubes. Based on the Monkhorst-Pack scheme,¹⁸ $1 \times 1 \times 5$ k mesh was used along the nanotube axis. In the density of states (DOS) calculation, the k mesh was increased to $1 \times 1 \times 12$.

Depending on the strength of adsorbate and surface interactions, one usually distinguishes between the two adsorption processes, chemisorption and physisorption. Chemisorption is due to covalent bond formation, while physisorption is a weak interaction which is dominated by the van der Waals (vdW) forces. While DFT performs well for short-range interactions, it is well known that the approximations used in DFT do not consider the van der Waals interactions accurately, usually the LDA overestimate binding energies, while the GGA underestimate binding energies. For the physisorption system, it is important to consider long-range interaction forces such as van der Waals interaction because these forces have the same magnitude as the weak chemical forces. In this paper, the contribution of van der Waals non-bonded interaction to the binding energy was also considered in a similar way as Dag *et al.*¹² The van der Waals attractive forces are calculated by Lenard-Jones 12-6-type expression, $E_{\text{vdw}}^{\text{LJ}} = AR^{-12} - BR^{-6}$, using the DREIDING force field¹⁹ as implemented in CERIUS2. The E_{vdw} listed in Table I is defined as $E_{\text{vdw}} = E_{\text{vdw}}(\text{BNNT}+\text{O}_2) - E_{\text{vdw}}(\text{BNNT}) - E_{\text{vdw}}$.

In this calculation, the adsorption energy is defined as $E_a = E_{(\text{BNNT}+\text{O}_2)} - E_{\text{BNNT}} - E_{\text{O}_2}$, where $E_{(\text{BNNT}+\text{O}_2)}$ is the total energy of the fully relaxed O₂-(5,5) BNNT adsorption system, and E_{BNNT} and E_{O_2} are energies of two isolated systems, respectively, i.e., clean (5,5) BNNT and O₂ molecule. By definition, a negative value of E_a corresponds to exothermic adsorption. The binding energies include both short-term and long-term interactions $E_b = E_{\text{vdw}} + E_a$. In our paper, the absolute magnitude of the physisorption energies are less than 0.1 eV (~ 10 kJ/mol), whereas the chemisorption energies are around 1 eV (~ 100 kJ/mol).

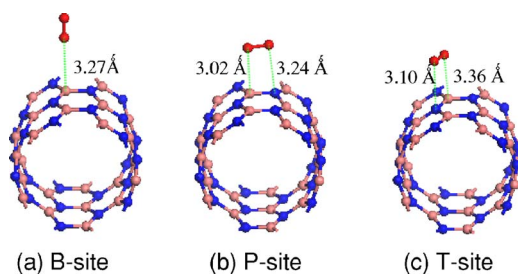


FIG. 1. (Color online) Optimized configurations for O₂ adsorbed on (5,5) BNNT: (a) B site, (b) P site, and (c) T site.

III. RESULTS AND DISCUSSION

A. Oxygenation of pristine (5,5) BNNTs

1. Physical adsorption of O₂ molecules

In order to investigate the physical adsorption of O₂ molecule on the wall of (5,5) BN nanotube, four adsorption sites are considered in our work. Figure 1 shows different O₂ adsorption configurations, with the molecular axis of O₂ being either vertical to the tangent plane of BNNT surface, adsorbing on the boron atom (B site) or nitrogen atom (N site), or parallel (slightly tilted) to the latitudinal B-N bond (P site) or zigzag B-N bond (T site). The singlet ($^1\Delta_g$) and triplet states ($^3\Sigma_g^-$) were considered in the spin-polarized calculations. The corresponding adsorption energies and equilibrium O₂-tube distance are listed in Table I. Results show that the triplet state is the ground state of the system. The triplet O₂ molecule is found to bind weakly on the exterior surface of nanotube with small exothermic adsorption energies when its bond axis is vertical to the plane of the BN wall, with large O₂-tube equilibrium distance > 3.0 Å. This means that there will be a net magnetic moment of $\sim 2\mu_B$ for O₂-BNNT per unit cell because of the triplet state of oxygen. However, when the bond axis is parallel to the plane of the BN wall, the adsorption energy is endothermic. Inclusions of van der Waals bonding gives a small exothermic binding energy, but this is not sufficient to prevent spontaneous desorption at room temperature.

For O₂ adsorption on B site, the excitation energy from triplet $^3\Sigma_g^-$ to spin-polarized singlet is only 435 meV, which is substantially underestimated in comparison with the experimental value of 0.98 eV for the $^3\Sigma_g^-$ to $^1\Delta_g$ excitation.²⁰ This is because the spin-polarized DFT calculation for singlet O₂ lead to “spin contamination,” which significantly lowers the energy of the singlet O₂.²¹ However, the energy difference calculated here between triplet $^3\Sigma_g^-$ and spin-restricted systems is 925 meV, similar to the experimental excitation energy. Hence, in the following studies the singlet state is treated as a closed-shell system, and the spin-restricted DFT calculation is used to model the singlet state.

2. Electronic properties of defect-free (5,5) BNNT with O₂ molecule on the tube wall

The electronic structures of pristine (5,5) BNNT with a single O₂ molecule adsorbing on the B site of the tube wall are investigated in this section. The band structures of the bare (5,5) BNNT, as well as O₂-physisorbed BNNT at the

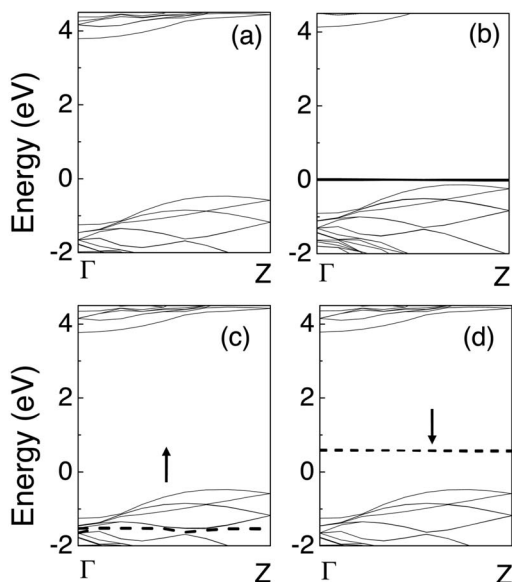


FIG. 2. Electronic band structure of (5,5) BNNT: (a) spin-unpolarized pure BNNT and (b) spin-unpolarized BNNT with O_2 adsorbed on B site. The O_2 -derived $pp\pi^*$ states are denoted as the bold solid lines overlapping with Fermi level. [(c) and (d)] Spin-triplet BNNT with O_2 adsorbed on B site. The bold dashed lines in (c) are O_2 -derived $pp\pi^*$ spin-up \uparrow states, and the bold dashed lines in (d) are O_2 -derived $pp\pi^*$ spin-down \downarrow states. The zero energy is the Fermi level.

triplet state, are shown in Fig. 2 where Fermi level is taken as zero energy. The plot in Fig. 2(a) shows that bare (5,5) BNNT is a semiconductor with an indirect band gap of 4.26 eV, consistent with previous theoretical calculations.²² For spin-unpolarized calculation, the O_2 -derived $pp\pi^*$ states overlap with the Fermi level in Fig. 2(b). However, for spin-polarized calculation, it can be seen that the O_2 -derived antibonding $1\pi_g$ states split into two spin-up states and two spin-down states; the spin-up states fall inside the valence band and occur at ~ -1.6 eV in Fig. 2(c), while the empty spin-down states are located at 0.55 eV above Fermi level at the Γ point in Fig. 2(d). For all single O_2 -BNNT systems, regardless of the adsorption sites (B, N, P, or T adsorption sites), a gap of ~ 1 eV opens up between the upper valence band and the empty spin-down states of oxygen; hence, the hole-doping picture, where ionization of the acceptor states take place readily due to small energy barrier for charge transfer from valence band, is not valid here.

B. Adsorption of O_2 on carbon-doped (5,5) BNNT

Previous theoretical studies indicated that C_B defect, where carbon substituted for a boron site, occurs in N-rich growth condition, while C_N defect occurs in B-rich growth condition.²³ In this work, both types of defects are considered. After optimization, the carbon substitutional atom is slightly displaced outward at both defect sites. Upon relaxation, the total energy is lowered by 0.27 eV for BNNT- C_N system and 0.30 eV for BNNT- C_B system, respectively. For C_N defect, the average C-B bond length increases to

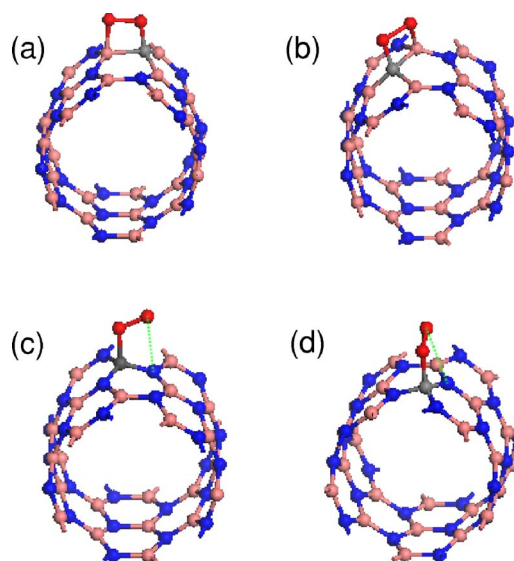


FIG. 3. (Color online) Optimized configurations of O_2 chemisorbed on C_N or C_B defect site of (5,5) BNNT: (a) C_N defect, P orientation, (b) C_N defect, T orientation, (c) C_B defect, P orientation, and (d) C_B defect, T orientation.

1.504 Å. However, for BNNT with C_B defect, the average C-N distance is shortened by 0.035 Å compared to the B-N distance in pristine BNNT (1.448 Å).

In order to investigate the influence of C defect on the reactivity of the (5,5) BN tube with O_2 , two adsorption orientations are selected. Similar to the pristine nanotube cases, the O_2 molecule is located above the latitudinal (P site), zig-zag C-B bond site, or C-N bond site (T site). The optimized configurations are displayed in Fig. 3, and the corresponding adsorption energy and geometry parameters are listed in Table II. As the presence of the carbon defect contributes one unpaired electron, the spin-doublet state is the ground state for clean carbon-doped BNNT system. Various possible spin states of the adsorption systems after the adsorption of oxygen molecule include singlet, doublet, triplet, and quartet states. In this work, the discussion will mainly focus on the ground state system.

It is found that O_2 can enter into stable chemisorption state on both C_N and C_B defect sites when it is adopting the P or T adsorption configuration, although on pristine BN nanotube walls shown earlier, only physisorption states are obtained. Calculation shows that the singlet state is the ground state for the chemisorbed O_2 on C_N defect site with adsorption energy of -1.10 eV for O_2 adopting the T configuration. At C_N defect site, as shown in Figs. 3(a) and 3(b), the chemisorbed O_2 molecule bonds with the underlying C-B bond to attain a bond distance (d_{B-O}) of 1.519 (or 1.694 for P) Å and d_{C-O} of 1.413 (or 1.442 for P) Å, forming a four-member ring. The strong chemical interaction elongates the O-O distance from 1.24 to 1.467 (or 1.390 for P) Å; the underlying C-B bond length has also increased by ~ 0.19 Å. The consequence of the spin pairing means that the localized magnetism due to doublet spin state of the carbon-doped BN nanotube is lifted, and the system become diamagnetic following oxygen chemisorption.

In the case of chemisorbed O_2 on C_B defect, the doublet state is the ground state, and adsorption energies of -1.36

TABLE II. Adsorption energies and geometry parameters for O₂ molecule adsorbed on the C_N or C_B defect of (5,5) BN nanotube. C_N defect: (5,5) BNNT with C atom substituting N atom. C_B defect: (5,5) BNNT with C atom substituting B atom. $d_{C-B(N)}$: the bond length of C–B in (5,5) BNNT with C_N defect or the bond length of C–N in (5,5) BNNT with C_B defect. The value in the parentheses is the corresponding bond length in bare (5,5) BNNT with C_N or C_B defect.

Defect site	Spin state	E_a (eV)/O ₂	$d_{B(N)-O}$ (Å)	d_{C-O} (Å)	d_{O-O} (Å)	$d_{C-B(N)}$ (Å)
C _N –P	Singlet	–0.93	1.623	1.424	1.413	1.686
C _N –P	Doublet	–1.03	1.694	1.442	1.390	1.674 (1.531)
C _N –T	Singlet	–1.10	1.519	1.413	1.467	1.687 (1.498)
C _N –T	Doublet	–1.00	1.584	1.433	1.433	1.634
C _B –P	Singlet	–0.96	2.632	1.651	1.313	1.422
C _B –P	Doublet	–1.36	2.631	1.652	1.312	1.423 (1.422)
C _B –T	Singlet	–1.13	2.580	1.622	1.318	1.424
C _B –T	Doublet	–1.46	2.579	1.625	1.316	1.424 (1.426)

and –1.46 eV for P and T chemisorption configurations were obtained, respectively. At the C_B defect [Figs. 3(c) and 3(d)], O₂ bonded mainly with the C atom to attain a bond length of 1.652 (P) or 1.625 (T) Å, which is slightly larger than the length of typical C–O single bond (1.43 Å). The nonbonding interaction between O and N results in one unpaired electron left on oxygen; thus, the spin-doublet system is favorable when O₂ chemisorbed on C_B defect, with a d_{N-O} of ~2.6 Å, and the system remains magnetic.

The calculated band structures and DOS for bare (5,5) BNNT with C_N or C_B defects, as well as the same systems after oxygen chemisorption, are shown in Figs. 4 and 5, where the Fermi level is taken as the zero of energy. The BNNT-C_N is an electron-deficient structure compared to defect-free BNNT; thus, the acceptorlike impurity state ap-

pears near the top of valence-band (VB) in Fig. 4(a). The BNNT-C_B system in contrast is an electron-rich system; in this case, the donorlike impurity state appears near the conduction band edge in Fig. 5(a). In Fig. 4(a), it can be seen that C_N defect creates a half-filled band in the band gap crossing the Fermi level. The local DOS in Fig. 4(b) shows that the new peak at the edge of VB is mainly due to the *p* orbitals of the C defect. Calculations based on the spin-polarized doublet state, as displayed in Figs. 4(c) and 4(d), reveal that the C_N defect state splits into an occupied spin-up and an empty spin-down level around the Fermi level. The calculated exchange splitting energy is 0.69 eV in this case.

In Fig. 6, we present the band structure as well as total and partial DOS for the singlet O₂-chemisorbed (5,5) BNNT-C_N system. The chemisorbed O₂ which adopts the T

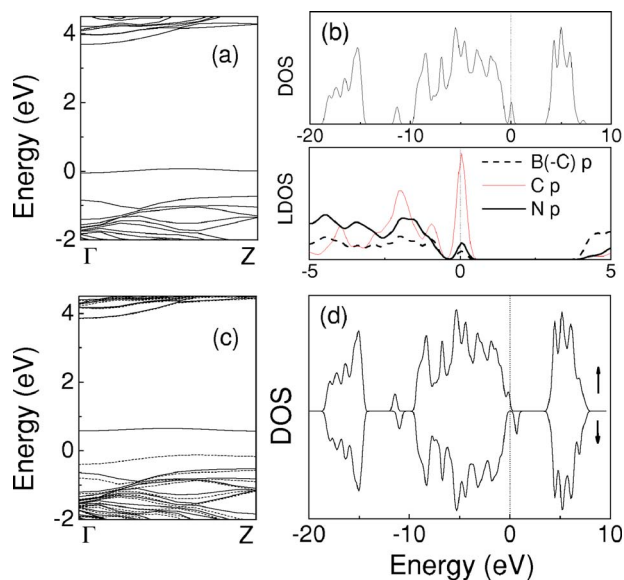


FIG. 4. (Color online) Electronic band structure (left) as well as total and partial DOS (right) of (5,5) BNNT with C_N defect: [(a) and (b)] spin singlet and [(c) and (d)] spin doublet. In (c), the solid lines denote spin-down ↓ states and the dashed lines represent spin up ↑ states. The zero energy is the Fermi level.

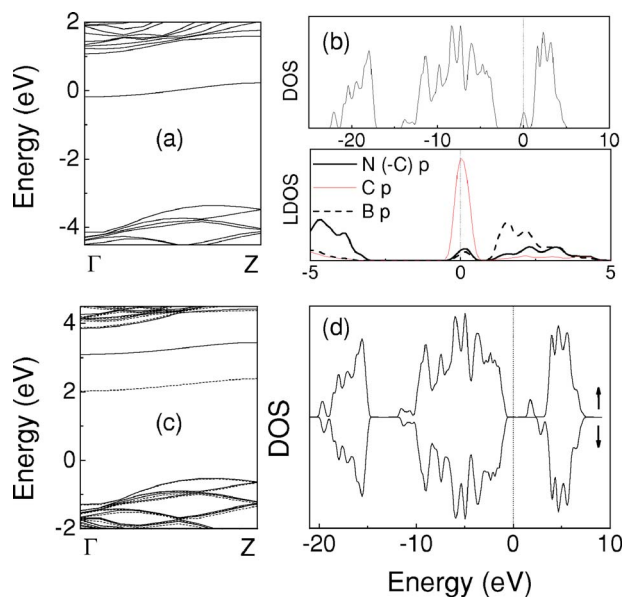


FIG. 5. (Color online) Electronic band structure (left) as well as total and partial DOS (right) of (5,5) BNNT with C_B defect: [(a) and (b)] spin singlet and [(c) and (d)] spin doublet. In (c), the solid lines denote spin-down ↓ states and the dashed lines represent spin up ↑ states. The zero energy is the Fermi level.

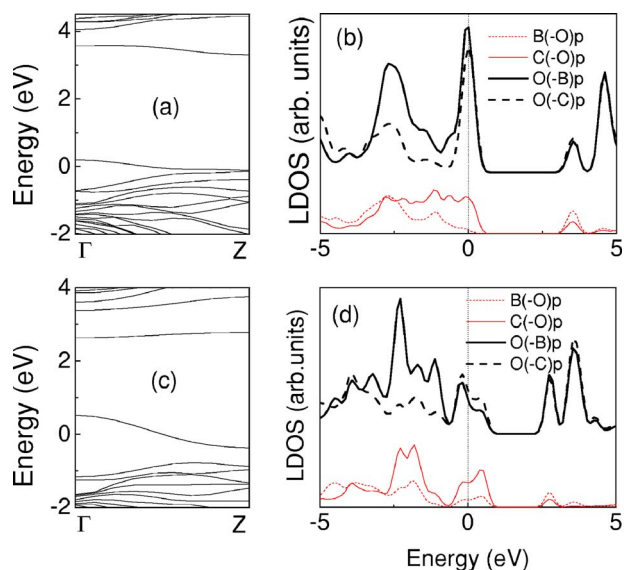


FIG. 6. (Color online) Electronic band structure as well as partial DOS for O_2 -BNNT- C_N chemisorption system spin singlet: [(a) and (b)] O_2 chemisorbed on C-B bond in P orientation and [(c) and (d)] O_2 chemisorbed on C-B bond in T orientation. The zero energy is the Fermi level.

configuration hybridizes with the B and C atoms and introduces a strongly dispersive “acceptorlike band” that crosses the Fermi level, as shown in Fig. 6(c). The Local DOS plots shown in Figs. 6(b) and 6(d) revealed that the bonding state crossing Fermi level are made up of hybridized O p , C p , and B p orbitals. Mulliken charge analysis reveals the transfer of $0.34e$ from boron atom to oxygen and $0.12e$ from carbon atom to oxygen. It can be inferred that the presence of a higher density of C_N defect sites will increase the coverage of chemisorbed oxygen, which in turn introduces more hybridized states in the gap near the Fermi level; these closely spaced states will merge into a half-filled band around the Fermi level, imparting metallicity on the BN nanotube.

For the electron-rich BNNT- C_B system, in the spin-doublet state, the C_B defect introduces an unoccupied (spin-down) level 0.77 eV below the conduction band edge, and an occupied (spin-up) level deep inside the band gap, with an energy separation between the two levels of 1.06 eV [see Figs. 5(c) and 5(d)]. Figures 7(a)–7(d) show that the chemisorption of O_2 in either P or T configuration introduces four deep levels in the band gap: two spin-up and one spin-down level below the Fermi level, and one spin-down level at approximately 0.76 eV above the Fermi level. Unlike the C_N case above, the dispersionless O-related lines indicate that the hybridization is mainly with C atoms, and not with N. The unoccupied spin-down states are separated from the valence band by more than 1 eV, so the hole doping picture is not valid here. Mulliken charge analysis revealed that there is no significant charge transfer between N and O, and $0.12e$ transferred between C and O.

The calculation results suggest that the walls of pristine BN nanotube are inert to molecular oxygen. First, the low binding energies obtained for all O_2 adsorption configurations in this work suggest that spontaneous desorption of O_2

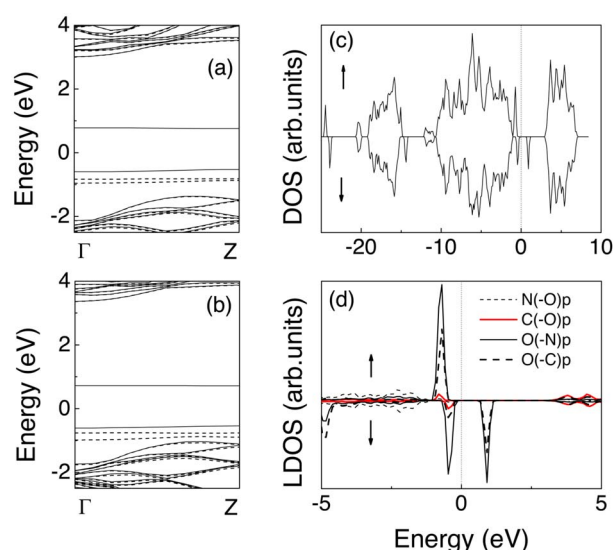


FIG. 7. (Color online) Spin-doublet electronic band structure as well as total and partial DOS for O_2 -BNNT- C_B chemisorption system: (a) band structure for BNNT- C_B with O_2 chemisorbed in P orientation, (b) band structure for BNNT- C_B with O_2 chemisorbed in T orientation, and [(c) and (d)] total and partial DOS for BNNT- C_B with O_2 chemisorbed in P orientation. The zero energy is the Fermi level. In (a) and (b), the solid lines denote spin-down \downarrow states and the dashed lines represent spin-up \uparrow states.

may occur at room temperature. Second, spin-polarized calculations show that there is no charge transfer between physisorbed O_2 and BN nanotube. One reason for the weak interactions between O_2 and BN nanotube is due to the electrostatic repulsion by nitrogen lone pairs. It is therefore unsurprising that the substitution of the nitrogen atom by carbon, to generate the C_N defect, allows the molecular oxygen to enter into a stable chemisorption state on top of the C–B bond. The mixing of the orbitals between oxygen, carbon, and boron in this case introduces a highly dispersive acceptorlike state which imparts metallic character on the BN nanotube. Therefore, a combination of carbon doping followed by exposure to air may be an effective way to tune the electronic properties of the insulating nanotube. Experimentally, a good evaluation of the validity of these theoretical results will be the controlled synthesis of BN nanotube under conditions of different chemical potentials (N- or B-rich environment), with intentional introduction of carbon impurity. The synthesized carbon-doped nanotubes can then be analyzed for their optical and electronic properties in an environment-controlled chamber where adsorption or desorption of oxygen can be carried out. It is also interesting that the magnetism of the doublet ground state induced by the carbon defect state is quenched by the adsorption of oxygen on the C_N defect, because the spin pairing in this case between the adsorbate and carbon-doped BN produces the singlet state as ground state. Conceptually, it is interesting to consider the possibility of generating a magnetic tube that can be switched on and off by gas exposure.

The influence of O_2 on the electronic properties of

carbon-doped BN depends on the nature of the defect site. On C_B -type defect, the effect of the nitrogen lone pair repulsion is present and interaction with oxygen is restricted to the carbon atom in the defect site. In the model with a single C_B defect and one chemisorbed oxygen molecule in the periodic unit cell, there is no evidence of p doping because the C-O impurity states are situated deep in the gap away from the band edges. Nonetheless, the optical properties of these nanotubes should be affected because transitions between these well-separated oxygen-induced impurity states will give rise to new peaks in UV absorption spectra or cause a redshift of the absorption peak. These impurity states will give rise to new bound states in the band gap which will change the optical response of the material. Zhi *et al.* showed recently that ultraviolet-visible absorption spectra of BN nanotube can be changed by surface chemical functionalization.²⁴ Increasing the concentration of these functional groups allows the overlapping of local molecular orbitals, producing an increase in the density of impurity states, consequently narrowing the band gap and imparting metallicity. It is plausible that a higher concentration of C_B defect will allow the neighboring adsorbed oxygen with unpaired

spins to interact laterally and cause a larger energy dispersion of the impurity states.

IV. CONCLUSIONS

Our computer simulation studies reveal that pristine BN nanotube is inert to molecular oxygen. However, BN nanotube with C_N or C_B defect allows O_2 to form stable chemisorption states, which affects the magnetic, optical, and electronic properties of the nanotube. Within the environment of the unit cell, the chemisorption of O_2 on C_N defect forms a strongly dispersive acceptorlike state above the valence band, imparting metallic character on the electronic properties of the nanotube. The chemisorption of O_2 on C_B defect, however, introduces deep gap states; consequently, the hole-doping effect is absent. The difference between chemisorption on the C_N or C_B defect is due to the presence or absence of nitrogen atom near the defect site in question because the presence of lone pair repulsion changes the nature of bonding and spin polarization with the chemisorbed oxygen. Finally, the introduction of impurity states in the gap regions will affect the optical properties of the BN nanotube.

*Author to whom correspondence should be addressed; FAX: (65) 67791691; electronic address: chmlhkp@nus.edu.sg

¹R. Ma, Y. Bando, T. Sato, and K. Kurashima, *Chem. Phys. Lett.* **350**, 434 (2002).

²R. Ma, Y. Bando, H. W. Zhu, T. Sato, C. Xu, and D. Wu, *J. Am. Chem. Soc.* **124**, 7672 (2002).

³N. Sai and E. J. Mele, *Phys. Rev. B* **68**, 241405(R) (2003).

⁴A. Rubio, J. L. Corkill, and M. L. Cohen, *Phys. Rev. B* **49**, 5081 (1994).

⁵K. H. Khoo, M. S. C. Mazzoni, and S. G. Louie, *Phys. Rev. B* **69**, 201401(R) (2004).

⁶A. Star, V. Joshi, S. Skarupo, D. Thomas, and J.-C. P. Gabriel, *J. Phys. Chem. B* **110**, 21014 (2006); S. Heinze, J. Tersoff, R. Martel, V. Derycke, J. Appenzeller, and Ph. Avouris, *Phys. Rev. Lett.* **89**, 106801 (2002).

⁷K. A. Park, Y. S. Choi, Y. H. Lee, and C. Kim, *Phys. Rev. B* **68**, 045429 (2003).

⁸J. Zhang, K. P. Loh, S. W. Yang, and P. Wu, *Appl. Phys. Lett.* **87**, 243105 (2005).

⁹P. G. Collins, K. Bradley, M. Ishigami, and A. Zettl, *Science* **287**, 1801 (2000).

¹⁰A. Kleinhammes, S.-H. Mao, X.-J. Yang, X.-P. Tang, H. Shimoda, J. P. Lu, O. Zhou, and Y. Wu, *Phys. Rev. B* **68**, 075418 (2003).

¹¹S.-H. Jhi, S. G. Louie, and M. L. Cohen, *Phys. Rev. Lett.* **85**,

1710 (2000).

¹²S. Dag, O. Gülseren, T. Yildirim, and S. Ciraci, *Phys. Rev. B* **67**, 165424 (2003).

¹³R. Q. Wu, L. Liu, G. W. Peng, and Y. P. Feng, *Appl. Phys. Lett.* **86**, 122510 (2005).

¹⁴G. Kresse and J. Hafner, *Phys. Rev. B* **48**, 13115 (1993); **49**, 14251 (1994).

¹⁵P. E. Blochl, *Phys. Rev. B* **50**, 17953 (1994).

¹⁶G. Kresse and D. Joubert, *Phys. Rev. B* **59**, 1758 (1999).

¹⁷J. P. Perdew and Y. Wang, *Phys. Rev. B* **45**, 13244 (1992).

¹⁸H. J. Monkhorst and J. D. Pack, *Phys. Rev. B* **13**, 5188 (1976).

¹⁹S. L. Mayo, B. D. Olsafson, and W. A. Goddard III, *J. Phys. Chem.* **94**, 8897 (1990).

²⁰G. Herzberg, *Molecular Spectra and Molecular Structure: Spectra of Diatomic Molecules*, 2nd ed. (van Nostrand Reinhold, Toronto, 1950), Vol. 1.

²¹S.-P. Chan, G. Chen, X. G. Gong, and Z.-F. Liu, *Phys. Rev. Lett.* **90**, 086403 (2003).

²²H. J. Xiang, J. Yang, J. G. Hou, and Q. Zhu, *Phys. Rev. B* **68**, 035427 (2003).

²³T. M. Schmidt, R. J. Baierle, P. Piquini, and A. Fazzio, *Phys. Rev. B* **67**, 113407 (2003).

²⁴C. Zhi, Y. Bando, C. Tang, and D. Golberg, *Phys. Rev. B* **74**, 153413 (2006).